HELLS inhibits autophagy-dependent ferroptosis in nasopharyngeal carcinoma by modulating the Nrf2/HO-1/GPX4 pathway

CHENGXUN JIN[1], JINQIU LI[1], SIQI HAN[1], CHAOLUOMENG BAI[2], JINGPU YANG[1] and ZONGGUI WANG[1]

[1]Department of Otolaryngology, The Second Hospital of Jilin University, Changchun, Jilin 130000, P.R. China;
[2]Department of Otolaryngology, Xing'an League People's Hospital, Ulanhot, Inner Mongolia Autonomous Region 137400, P.R. China

Received May 16, 2025; Accepted November 25, 2025

DOI: 10.3892/ijmm.2026.5788

Abstract. The present study aimed to elucidate the role of lymphoid-specific helicase (HELLS) in autophagy-dependent ferroptosis in nasopharyngeal carcinoma (NPC) cells and associated mechanisms. Bioinformatics analyses were conducted to identify the key gene. Gene knockout was accomplished through short-hairpin RNA transfection. Reverse transcription-quantitative polymerase chain reaction was conducted to evaluate mRNA expression, whereas protein expression was assessed through immunohistochemistry and western blotting. Furthermore, cell proliferation, migration, invasion and apoptosis were investigated via the Cell Counting Kit-8, Transwell and flow cytometry assays. Glutathione (GSH), malondialdehyde (MDA) and Fe^{2+} were quantified using commercial reagent kits. Reactive oxygen species (ROS) were assessed through immunofluorescence. Additionally, a tumor xenograft mouse model was employed for *in vivo* validation. HELLS, upregulated in human NPC tissue, was selected from 15 candidate genes. HELLS knockout resulted in decreased proliferation, migration and invasion while promoting apoptosis and autophagy in NPC/HK1 cells. Furthermore, the administration of ferroptosis and autophagy agonists increased the levels of MDA, Fe^{2+}, 4-hydroxynonenal and ROS, as well as the expression of acyl-CoA synthetase long-chain family member 4 and prostaglandin-endoperoxide synthase 2. Conversely, GSH levels decreased. These observed trends can be reversed by ferroptosis and autophagy inhibitors. HELLS knockout also caused the downregulation of nuclear factor-erythroid 2-related factor 2 (Nrf2), heme oxygenase-1 (HO-1) and glutathione peroxidase 4 (GPX4), which can be modulated by Nrf2 agonist. In *in vivo* experiments, HELLS expression reduction inhibited tumor growth and the expression of Nrf2, HO-1 and GPX4 while promoting autophagy. In conclusion, HELLS activates the Nrf2/HO-1/GPX4 pathway, which inhibits autophagy-dependent ferroptosis in NPC cells, thereby promoting NPC progression.

Correspondence to: Professor Jingpu Yang or Dr Zonggui Wang, Department of Otolaryngology, The Second Hospital of Jilin University, 4026 Yatai Street, Nanguan, Changchun, Jilin 130000, P.R. China
E-mail: yangjingpu@jlu.edu.cn
E-mail: zonggui@jlu.edu.cn

Key words: lymphoid-specific helicase, autophagy-dependent ferroptosis, nasopharyngeal carcinoma, nuclear factor-erythroid 2-related factor 2/heme oxygenase 1/glutathione peroxidase 4 pathway

Introduction

Nasopharyngeal carcinoma (NPC) is an elusive epithelial malignancy that arises in the nasopharynx and is characterized by significant geographic variations in its incidence. The analysis of epidemiological trends over the past decade revealed a gradual decline in the incidence of NPC (1). Nevertheless, in Southeast Asia and East Asia, particularly in the south of China, the incidence of NPC remains significantly higher than those in other regions globally (2), necessitating ongoing vigilance from the Chinese medical community. Although various etiological factors and key molecules implicated in the onset and metastasis of NPC have been identified (3-6), the current understanding of these factors and their associated mechanisms is insufficient to completely elucidate the pathogenesis of NPC. Consequently, conducting further mechanistic investigations of NPC is an urgent requirement to deepen our understanding of the disease and support its application in clinical interventions.

Since the identification of ferroptosis as an emerging form of programmed cell death (PCD) in 2012 (7), it has attracted significant attention from the scientific community. This form of cell death is heavily dependent on iron, which causes excessive reactive oxygen species (ROS) accumulation and, consequently, dangerously high levels of lipid peroxides (8). Since its discovery, ferroptosis has been closely associated with cancer. It was first induced and characterized in human fibrosarcoma cells expressing oncogenic Ras protein following treatment with erastin and Ras-selective lethal small molecule 3 (7). Then, a particular type of PCD was acknowledged to facilitate the elimination of cancer cells, with evidence demonstrating that induced ferroptosis effectively inhibits head

and neck cancers (9,10), including NPC (11-13). A previous study identified that ferroptosis is dependent on autophagy and is characterized by excessive activation of autophagic mechanisms (14). Autophagy-dependent ferroptosis also serves as a pivotal regulator in the inhibition of cancer progression. In lung adenocarcinoma (15), pancreatic carcinoma (16) and triple-negative breast cancer (17), key genes or crucial bioactive compounds associated with autophagy-dependent ferroptosis have been identified. Nevertheless, the mechanisms underlying autophagy-dependent ferroptosis in NPC remain unclear. Therefore, the present study aimed to identify the genes associated with autophagy-dependent ferroptosis in NPC and explore the regulatory mechanisms involved.

The regulatory mechanisms of ferroptosis are generally diverse and intricate. To date, numerous signaling pathways that regulate ferroptosis have been identified. Among these, the nuclear factor-erythroid 2-related factor 2 (Nrf2)/heme oxygenase (HO)-1/glutathione peroxidase 4 (GPX4) signaling pathway has attracted considerable research interest. This pathway has been recognized not only as a potential therapeutic target for malignant tumors occurring in various body regions, including breast (18), tongue (19), liver (20) and ovary (21) but also as being linked to various diseases associated with ferroptosis (22). However, research on the potential significance of this pathway in NPC remains limited.

The present study aimed to identify the key gene that regulates NPC and ferroptosis through bioinformatics analysis and an extensive review of the literature. Furthermore, *in vitro* and *in vivo* methodologies were employed to investigate the modulatory functions of this key gene in NPC and mechanisms associated with autophagy-dependent ferroptosis, thereby elucidating the potential of this gene as a therapeutic target for NPC.

Materials and methods

Bioinformatics analyses. The GSE12452 dataset, containing 31 NPC samples and 10 controls, was sourced from Gene Expression Omnibus (GEO; https://www.ncbi.nlm.nih.gov/geo/). Ferroptosis-related genes (FRGs) were downloaded from the FerrDB database (http://www.zhounan.org/ferrdb/current/). Differentially expressed genes (DEGs) between NPC and healthy controls were identified using the limma package in R with criteria of $|\log2FC| > 1.5$ and adjusted $P<0.05$ (23). Key genes associated with NPC and ferroptosis were then determined by intersecting DEGs with FRGs.

To further verify whether the expression level of lymphoid-specific helicase (HELLS) is higher in NPC, single-cell RNA sequencing data was downloaded from the 10X Genomics platform in the GSE120926 dataset, which includes 16 primary NPC tumors and 7 non-malignant rhinitis biopsies. The Read 10X function from the Seurat package (version 4.30) was utilized to load the data. Cells were filtered to retain those containing between 200-6,000 detected genes and with a mitochondrial gene expression ratio of <10%, resulting in a final dataset of 101,110 cells. Data normalization was performed using Log Normalize, followed by identification of highly variable genes with the Find Variable Features function (n features=3,000), and the Scale Data function to standardize gene expression levels within each cell to a mean of 0 and variance of 1, regressing out technical covariates [var.to. regress=c ('n Count_ RNA', 'percent. Mito')]. Following dimensionality reduction via principal component analysis, batch effects across different samples were corrected using the Harmony package. A k-nearest neighbor graph was constructed with the Find Neighbors function, and cells were clustered using the Find Clusters function (resolution=0.1). Finally, cell types were annotated based on marker genes curated in the Cell Marker 2.0 database.

Transcriptome data of 12 pairs of NPC tissues with high and low intratumoral bacterial loads were downloaded from the GSE189642 dataset in the GEO database, with expression values presented as FPKM. The expression levels of HELLS were extracted from all samples, and the Wilcoxon rank-sum test was used to calculate the differences in HELLS expression between the high and low intratumoral bacterial load groups.

Patients. The present study included five patients diagnosed with NPC who received treatment at the Department of Otolaryngology, The Second Hospital of Jilin University, between March 2023 and March 2024. Inclusion criteria for patient enrollment were as follows: (i) Confirmed diagnosis of NPC by pathological examination; (ii) aged 18 years or older; and (iii) clear consciousness. Exclusion criteria were: (i) Comorbidity with other major malignant tumors or severe diseases; (ii) presence of mental or cognitive disorders; and (iii) inability to communicate normally. Pathological specimens were obtained through endoscopic nasopharyngeal biopsy for confirming the diagnosis of NPC and endoscopic resection of lesions to remove localized tumor tissue. Tumor and paracancerous normal tissue (the distance from the tumor tissue was 2-3 cm) samples of suitable sizes were gathered intraoperatively and subsequently preserved at -80˚C. Waiver of informed consent was approved by the Medical Ethics Committee of The Second Hospital of Jilin University, which also granted ethical approval for this study (approval no. 2023-301; Changchun, China). Information of clinical patients (including sex and age) is presented at Table I.

Cell culture. Human NPC cell lines NPC/HK-1 (cat. no. IM-H533) and C666-1 (cat. no. IM-H432) and nasopharyngeal epithelial cell line NP69 (cat. no. IM-H435; all from Xiamen Immocell Biotechnology Co., Ltd.) were maintained in a humid and aseptic environment at 37˚C with 5% CO_2. NPC/HK-1 and NP69 cell lines were cultured in RPMI-1640 medium (Corning, Inc.), added with 10% fetal bovine serum (FBS; Sijiqing; https://www.hzsjq.com/) and penicillin-streptomycin solution (Biosharp Life Sciences). By contrast, C666-1 cells were cultivated in DMEM with 15% FBS and a solution containing both aforementioned antibiotics.

Cell transfection. Cells were plated in a 96-well plate at a uniform concentration of $3x10^4$ cells per well and cultivated for 24 h. The minimum puromycin concentration that can eliminate cells was initially determined. Following this, cell transfection was conducted using Lipofectamine 2000 (Thermo Fisher Scientific, Inc.). The mixture comprising the transfection reagent and plasmid DNA (0.3 μg per well, 1 μg/l) was prepared and subsequently administered to cells. Gene expression was assessed following a 48-h culture at 37˚C with 5% CO_2. The short hairpin (sh) RNA sequences were as

Table I. Clinicopathological characteristics of the patients from which the samples were derived, including sex, pathological type, clinical stage and clinical status.

Patients with NPC	Sex	Age, years	Pathological type	Clinical stage	Clinical status	Specimen collection method
1	Male	52	Undifferentiated non-keratinizing carcinoma	III	Initial treatment	Endoscopic biopsy
2	Female	50	Undifferentiated non-keratinizing carcinoma	III	Initial treatment	Endoscopic biopsy
3	Male	46	Undifferentiated non-keratinizing carcinoma	II	Initial treatment	Endoscopic biopsy
4	Male	61	Differentiated non-keratinizing carcinoma	IVA	Recurrence	Endoscopic biopsy
5	Female	58	Undifferentiated non-keratinizing carcinoma	II	Initial treatment	Endoscopic biopsy

NPC, nasopharyngeal carcinoma.

follows: sh-HELLS-1: CAGGAAAGAATTCCTAGAATG TATG; sh-HELLS-2: CCAGGAAAGAATTCCTAGAAT GTAT; and sh-HELLS-3: GCTGCACCAGGAAAGAATTCC TAGA; sh-negative control (NC): TTCTCCGAACGTGTC ACGT.

Cell treatment and group setting. To modulate ferroptosis, cells transfected with sh-NC and sh-HELLS sequences were treated for 24 h with either 10 μM of erastin (cat. no. HY-15763; MedChemExpress) or a combination of 10 μM of Erastin and 2 μM ferrostatin-1 (Fer-1; cat. no. HY-100579; MedChemExpress) (11,24). Furthermore, to investigate apoptosis-dependent ferroptosis, cells were initially stimulated with erastin and subsequently treated with either 500 nM rapamycin (Rapa; cat. no. HY-10219; MedChemExpress) or 5 mM 3-methyladenine (3-MA; cat. no. HY-19312; MedChemExpress) for 24 h (25,26). To investigate whether autophagy-dependent ferroptosis was regulated through the Nrf2/HO-1/GPX4 signaling pathway, cells were initially stimulated with erastin and subsequently treated with 1 μM ML334 (cat. no. HY-110258; MedChemExpress) for 24 h.

Cell proliferation assay. Cells were seeded into 96-well plates at a defined cell density of $5x10^3$ cells per well and cultured at various time intervals. Upon achieving the defined treatment period, the medium was removed, and 10 μl per well of freshly prepared Cell Counting Kit-8 reagent (Kermey; http://www.jacksenbio.com/) was supplied to the cells and incubated at 37˚C for 1 h. The OD value at 450 nm was measured promptly.

Cell apoptosis assay. Cells were suspended in 1X binding buffer, and Annexin V-mCherry and GreenNuc™ Caspase-3 Substrate (all three components of the Caspase-3 Activity and Apoptosis Detection Kit for Live Cell; cat. no. C1077M; Beyotime Institute of Biotechnology) were subsequently added. Following gentle mixing, the mixture was incubated in the dark for 30 min to facilitate staining. Subsequently, 1X binding buffer was added to halt the staining process, and the thoroughly mixed cell suspension was analyzed employing a BD FACSCalibur™ flow cytometer (Becton, Dickinson and Company). Data analysis was performed with FlowJo software (version 10.8.1; FlowJo LLC).

Transwell assay. Cell migration and invasion were assessed using the Transwell assay with an 8-μm pore size. Specifically, in the migration measurement, cells were inoculated into the upper chamber at a density of $5x10^5$ cells per well, whereas the lower chamber was filled with the medium containing 15% FBS. In the invasion assay, cells were placed in the same part, which was pretreated with Matrigel (Corning, Inc.) at 37˚C for 60 min, and the lower chamber was filled with the same complete medium. Following 24-h incubation at 37˚C, the cells that stayed in the upper part were removed. Conversely, the cells that migrated or invaded through the filter pores were fixed with 100% methanol at room temperature for 30 min, stained with 0.1% crystal violet (cat. no. BL802A; Biosharp Life Sciences) at room temperature for 15 min, and images were captured.

Glutathione assay. Glutathione (GSH) concentrations within the cells were evaluated using the reduced GSH assay kit (cat. no. A006-2-1; Nanjing Jiancheng Bioengineering Institute), following the guidelines provided by the manufacturer.

Malondialdehyde (MDA) assay. The MDA levels were assessed using a lipid peroxidation MDA assay kit (cat. no. S0131S; Beyotime Institute of Biotechnology) based on the manufacturer's instructions.

Ferrous iron assay. Cell ferrous iron fluorometric assay kit (cat. no. E-BC-F101; Elabscience Biotechnology, Inc.) was employed to determine Fe^{2+} concentrations.

ROS assay. The immunofluorescence technique facilitates the direct and visual detection of ROS levels. In this procedure, the cells were washed twice with serum-free culture medium and subsequently incubated in the dark at 37˚C for 25 min with

a 2', 7'-dichlorodihydrofluorescein diacetate working solution (DCFH-DA/serum-free culture medium=1:1,000). Following incubation, the cells were washed twice with serum-free culture medium to remove any intracellular unbound DCFH-DA and subsequently imaged using a fluorescence microscope.

Xenograft model. A total of 12 male Balb/c nude mice, obtained from Charles River Laboratories, were housed in a specific pathogen-free environment at 25˚C with a 12/12-h light/dark cycle, and provided with *ad libitum* access to food and water. The mice were allocated randomly into two groups (sh-NC and sh-HELLS, n=6). Each animal experimental procedure gained approval from Institutional Animal Care and Use Committee of Jilin University (approval no. SY202406011; Changchun, China). A total of $5x10^6$ cells transfected with sh-HELLS or sh-NC plasmids were injected subcutaneously into the dorsal region of each nude mouse, respectively. Following cell implantation, tumor diameter was measured every 3 days to construct a tumor growth curve. On day 19 post-implantation, the mice were euthanized by intravenous injection of pentobarbital sodium at a dose of 150 mg/kg. Subsequently, the tumors were surgically excised, weighed and preserved for subsequent research.

Reverse transcription-quantitative polymerase chain (RT-qPCR) reaction. The TRIzol (Invitrogen; Thermo Fisher Scientific, Inc.) method was initially employed to extract the total RNA. Subsequently, a reverse-transcription assay was conducted to synthesize cDNA employing the TransScript II First-Strand cDNA Synthesis SuperMix (TransGen Biotech Co., Ltd.) following the manufacturer's instructions. ChamQ Universal SYBR qPCR master Mix (Vazyme Biotech Co., Ltd.) was used for RT-qPCR assays to assess gene expression, with thermocycling conditions as follows: Initial denaturation at 95.0˚C for 30 sec; followed by 40 cycles of denaturation at 95.0˚C for 10 sec, annealing and extension at 60.0˚C for 30 sec. Relative expression levels were quantified using the $2^{-\Delta\Delta Cq}$ method, with GAPDH as the normalization criterion (27). The primer sequences are presented in Table SI.

Western blot analysis. Radio immunoprecipitation assay buffer (Beyotime Institute of Biotechnology), supplemented with phenyl-methane-sulfonyl fluoride (PMSF) and protease inhibitor cocktail (100X), was initially used to obtain the total protein. Following the quantification of protein concentration utilizing a bicinchoninic acid (BCA) assay kit, total proteins (20 μg per lane) were separated via sodium dodecyl sulfate-polyacrylamide gel electrophoresis (SDS-PAGE) on a 10% acrylamide gel and subsequently transferred to polyvinylidene difluoride membranes (MilliporeSigma). Following blocking with 5% non-fat milk (prepared with 0.5 g milk powder in 10 ml TBS-T) at room temperature for 1 h, the membranes were incubated with primary antibodies (1:1,000) at 4˚C overnight, after which they were incubated with secondary antibodies (1:5,000). An enhanced chemiluminescence (ECL) kit (Beyotime Institute of Biotechnology) was employed to detect protein blots using a gel imaging system (Chemidoc XRS, Bio-Rad Laboratories, Inc.). Grayscale analysis of the protein bands was performed using ImageJ software (Version 1.8.0; National Institutes of Health). The antibodies included Lsh/HELLS (cat. no. A22289), Beclin 1 (cat. no. A21191), MAP1LC3A (cat. no. A12319), COX2/PTGS2 (cat. no. A3560), ACSL4 (cat. no. A22901), HO-1/HMOX1 (cat. no. A19062), GPX4 Rabbit mAb (cat. no. A11243; all from ABclonal Biotech Co., Ltd.), anti-4 hydroxynonenal (cat. no. ab48506), anti-Nrf2 antibody (cat. no. ab137550; both obtained from Abcam), horseradish peroxidase (HRP)-conjugated goat anti-rabbit IgG (cat. no. A0208) and HRP-conjugated goat anti-mouse IgG (cat. no. A0216; both purchased from Beyotime Institute of Biotechnology).

Immunohistochemistry. The tissue, which had been fixed with 4% buffered paraformaldehyde at room temperature for 6 h and dehydrated before paraffin embedding, was sectioned into ~5-μm-thick slices. The slides were then made transparent and dehydrated, and antigens were retrieved through immersion in boiled sodium citrate buffer (pH 6.0) for 10 min. Subsequently, a 0.5% Triton X-100 solution, prepared in Dulbecco's phosphate-buffered saline, was incubated with the slides for 20 min and then applied with a 3% H_2O_2 solution to eliminate endogenous peroxidases. Following a 30-min blocking period with a 5% bovine serum albumin (Beyotime Institute of Biotechnology) solution, the slides were incubated overnight with diluted primary antibody against Lsh/HELLS (1:100; cat. no. A22289; ABclonal Biotech Co., Ltd.) at 4˚C, then incubated for 30 min with HRP-conjugated goat anti-mouse IgG secondary antibody (1:50; cat. no. A0216; both purchased from Beyotime Institute of Biotechnology) and stained using a DAB kit (Beyotime Institute of Biotechnology). The staining results were then observed and imaged using a light microscope.

Co-immunoprecipitation (Co-IP). CO-IP assays for HELLS and Nrf2 were conducted using the Pierce® Co-IP Kit (cat. no. 26149; Thermo Fisher Scientific, Inc.) following the manufacturer's protocol. Briefly, protein lysates were prepared from HK-1 cells using PMSF buffer supplemented with a protease inhibitor cocktail. Centrifuge columns containing resin suspension were incubated with anti-HELLS antibody (1:100; cat. no. 11955-1-AP; Proteintech Group, Inc.) or anti-Nrf2 antibody (1:100; cat. no. 2221102; Zen Bio; https://www.zen-bio.cn/); rabbit IgG (1:100; cat. no. 30000-0-AP; Proteintech Group, Inc.) served as the negative control at 4˚C for 2 h. Protein lysates were then incubated with the antibody-loaded resin to capture target proteins at 4˚C overnight, which were eluted with elution buffer thereafter. The eluted proteins were separated by SDS-PAGE and subsequently analyzed by western blotting.

Statistical analysis. Statistical analyses were performed using GraphPad Prism 8.0 software (Dotmatics). Before conducting t-tests and one-way analysis of variance (ANOVA) on the experimental data, the homogeneity of variance assumption of the data was verified using the Homogeneity of Variance Test built into the software. Specifically, unpaired Student's t test was used for comparisons between two groups, while Welch's corrected t-test was applied if variance homogeneity was not satisfied. For comparisons among multiple groups, one-way ANOVA was used in combination with Tukey's post hoc test. Results are expressed as the mean ± standard deviation. $P<0.05$ was considered to indicate a statistically significant difference. All experiments were conducted in triplicate.

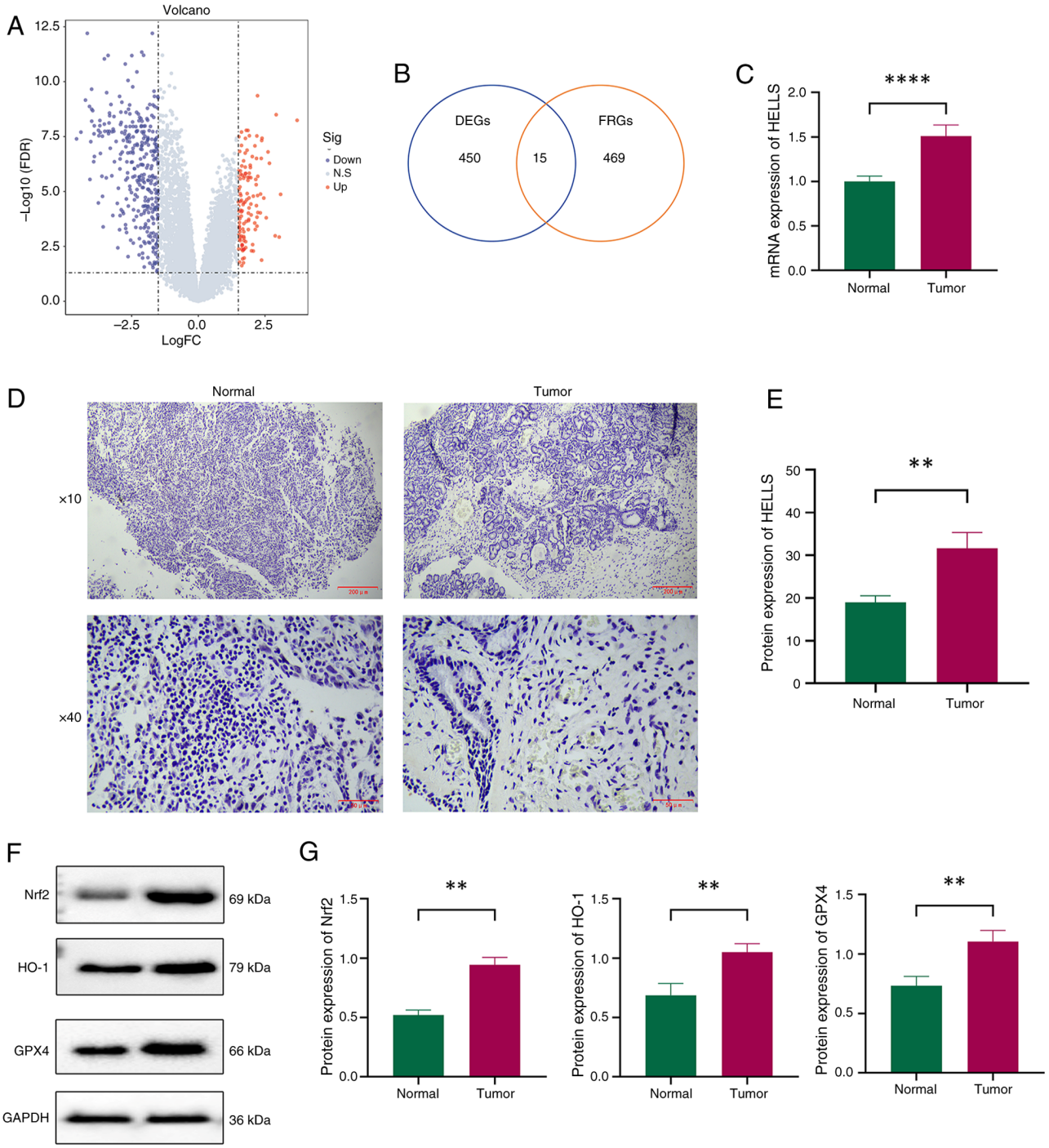

Figure 1. Identification and validation of the expression of the key gene HELLS in NPC. (A) Volcano plot illustrating DEGs identified through differential expression analysis. (B) Venn diagram of the interaction between DEGs and FRGs. (C) Relative mRNA expression levels of HELLS in NPC and paracancerous tissue (n=5). (D) Representative images depicting the immunohistochemical staining of HELLS in patients with NPC and paracancerous tissue. (E) Relative protein expression levels of HELLS in patients with NPC and paracancerous tissue. (F) The expression of Nrf2, HO-1 and GPX4 protein were detected using WB in NPC and adjacent. (G) Statistical analysis of Nrf2, HO-1 and GPX4 protein detected by WB. **P<0.01 and ****P<0.0001. HELLS, lymphoid-specific helicase; NPC, nasopharyngeal carcinoma; DEGs, differentially expressed genes; FRGs, ferroptosis-related genes; Nrf2, nuclear factor-erythroid 2-related factor 2; HO-1, heme oxygenase 1; GPX4, glutathione peroxidase 4; WB, western blotting.

Results

HELLS exhibits elevated expression in NPC. A total of 465 DEGs, comprising 125 upregulated and 331 down-regulated genes, were identified from the GSE12452 dataset (Fig. 1A). Additionally, a total of 484 FRGs were obtained from FerrDB (Table SII), and 15 DEGs associated with ferroptosis (FRDEGs) were obtained by the intersection between DEGs and FRGs (Fig. 1B and Table SIII). In the present study, HELLS was ultimately chosen from 15 FRDEGs for further investigation based on a thorough literature review (28-32) and alignment with research interests.

Following the official Seurat workflow, after performing dimensionality reduction and clustering on the cells, 9 major

cell types were ultimately obtained, including: Plasma B cells, B cells, plasmacytoid dendritic cells, myofibroblasts, endothelial cells, epithelial cells, T cells, natural killer cells and myeloid cells (Fig. S1A). The marker gene corresponding to each cell type are shown in Fig. S1B and C. Meanwhile, the expression level of HELLS in total cell was significantly higher in the primary tumor group ($P<2.2x10^{-16}$, Fig. S1D), and the expression level of HELLS in epithelial cells was also significantly higher in the primary tumor group ($P=3.82x10^{-8}$; Fig. S1E). To compare the expression levels of HELLS among different NPC subtypes, the GSE189642 dataset was obtained from the GEO database. The samples were grouped into high and low intratumoral bacterial load groups based on the degree of bacterial infiltration. The analysis results showed that the expression level of HELLS in the high intratumoral bacterial load group was significantly higher than that in the low load group (P=0.02), suggesting a positive association between HELLS expression and the degree of intratumoral bacterial infiltration (Fig. S1F).

Subsequently, the mRNA and protein expression levels of HELLS were validated by RT-qPCR and immunohistochemistry, respectively. As illustrated in Fig. 1C-E, both mRNA and protein expression levels of HELLS were significantly increased in the NPC tumor tissue in comparison with the adjacent non-cancerous tissue (P<0.01), thereby providing further evidence of the high expression of HELLS in NPC. Western blotting showed that Nrf2, HO-1 and GPX4 protein were significantly increased in NPC compared with adjacent tissue, suggesting that NPC tumor cells may escape ferroptosis and promote survival by activating this pathway (P<0.01, Fig. 1F and G).

HELLS promotes the progression of NPC in vitro. The selection of an appropriate cell line for research is of utmost importance. In alignment with the study's objectives, cell models were selected based on their HELLS expression. As demonstrated in Fig. 2A, HELLS expression was upregulated in NPC/HK1 and C666-1. Meanwhile, the same expression trend was observed at the protein level (Fig. 2B and C). Notably, the expression level of HELLS in the NPC/HK1 cell line was significantly higher than those in NP69 and C666-1 cell lines (P<0.01). Consequently, the NPC/HK1 was selected for further experimentation. Subsequently, HELLS was suppressed through the application of cell transfection.

The effect of HELLS gene knockout on NPC cells was subsequently investigated in detail. As revealed in Fig. 2D-F, the expression levels of both the HELLS gene and protein significantly decreased in the sh-HELLS group compared with those in the sh-NC group (P<0.01). The evaluation of cell proliferation capacity revealed that the sh-HELLS group demonstrated a significantly diminished proliferative ability in comparison with both the sh-NC and control groups (Fig. 2G; P<0.01). Furthermore, cell apoptosis analysis revealed that low HELLS expression significantly increased the apoptotic rate, which reached 12.13±0.92% (Fig. 2H and I; P<0.01). Subsequently, the migratory and invasive properties of the cells were evaluated. As illustrated in Fig. 2J and K, when compared with the control and sh-NC groups, the migratory abilities of sh-HELLS cells were significantly decreased (P<0.0001). Moreover, the invasive capabilities of sh-HELLS cells were significantly reduced (Fig. 2L and M; P<0.05). Furthermore, the assessment of autophagy markers revealed that HELLS knockout led to an increase in Beclin 1 expression levels and the LC3-II/LC3-I ratio (Fig. 2N-P; P<0.01), thereby providing evidence for an enhanced autophagic process. Concurrent with these analyses, the identical experimental procedures were replicated in the C666-1 cell line, which further validated the robustness and reproducibility of the aforementioned findings (Fig. S2).

HELLS suppresses ferroptosis. To evaluate the role of HELLS in ferroptosis, the ferroptosis agonist erastin and the inhibitor ferrostatin-1 (Fer-1) were administered to cells, and a comprehensive assessment of ferroptosis-related biomarkers (GSH, MDA, Fe^{2+} and ROS) was then conducted. In comparison with the sh-NC group, GSH levels were significantly reduced in the sh-HELLS group (P<0.05). Following treatment with erastin, GSH levels in the cells were significantly diminished compared with the untreated group (P<0.0001), whereas the subsequent administration of Fer-1 after erastin administration effectively reversed this outcome (Fig. 3A; P<0.0001). Subsequent analysis of MDA levels revealed a significant increase (P<0.05) following HELLS knockdown. Furthermore, the erastin group exhibited significantly high MDA levels, whereas treatment with Fer-1 resulted in a significant reduction of MDA levels in this context (Fig. 3B; P<0.0001). The results of Fe^{2+} concentration measurements closely align with those obtained for MDA. Specifically, under identical experimental conditions, the Fe^{2+} concentration in the sh-HELLS group was remarkably high compared with that in the sh-NC group (P<0.05). The findings also indicated that erastin facilitates the enhancement of Fe^{2+} accumulation, whereas Fer-1 appears to mitigate this phenomenon (Fig. 3C; P<0.0001). The evaluation of the three aforementioned indicators presented substantial evidence that HELLS significantly suppresses ferroptosis. Meanwhile, similar results were likewise observed in C666-1 cells (Fig. S3).

The ROS levels were further assessed, along with the expression levels of ferroptosis-associated genes and proteins. ROS levels significantly increased in the sh-HELLS group in comparison with those in the sh-NC group (P<0.01). This trend persisted following the administration of identical treatments with erastin and erastin in conjunction with Fer-1 (Fig. 3D and E; P<0.05). The expression levels of FRGs and proteins were consistent with the results of the assessment of various ferroptosis markers. RT-qPCR analyses revealed a significant upregulation of *ACSL4* and *PTGS2* genes following HELLS suppression (P<0.05). Additionally, erastin administration led to a significant increase in the expression of these genes (P<0.05). Conversely, the ferroptosis inhibitor Fer-1 significantly reversed this high expression trend (Fig. 3F and G; P<0.01). The protein expression patterns of these genes aligned with their respective gene expressions (Fig. 3H, J and K).

4-Hydroxynonenal (4-HNE) functions as a significant biomarker for ferroptosis-associated lipid peroxidation. Western blot analysis showed that 4-HNE levels accumulated in patterns consistent with the expression profiles of ACSL4 and PTGS2 across all cell groups (Fig. 3H and I; P<0.05), further supporting that HELLS significantly suppresses ferroptosis.

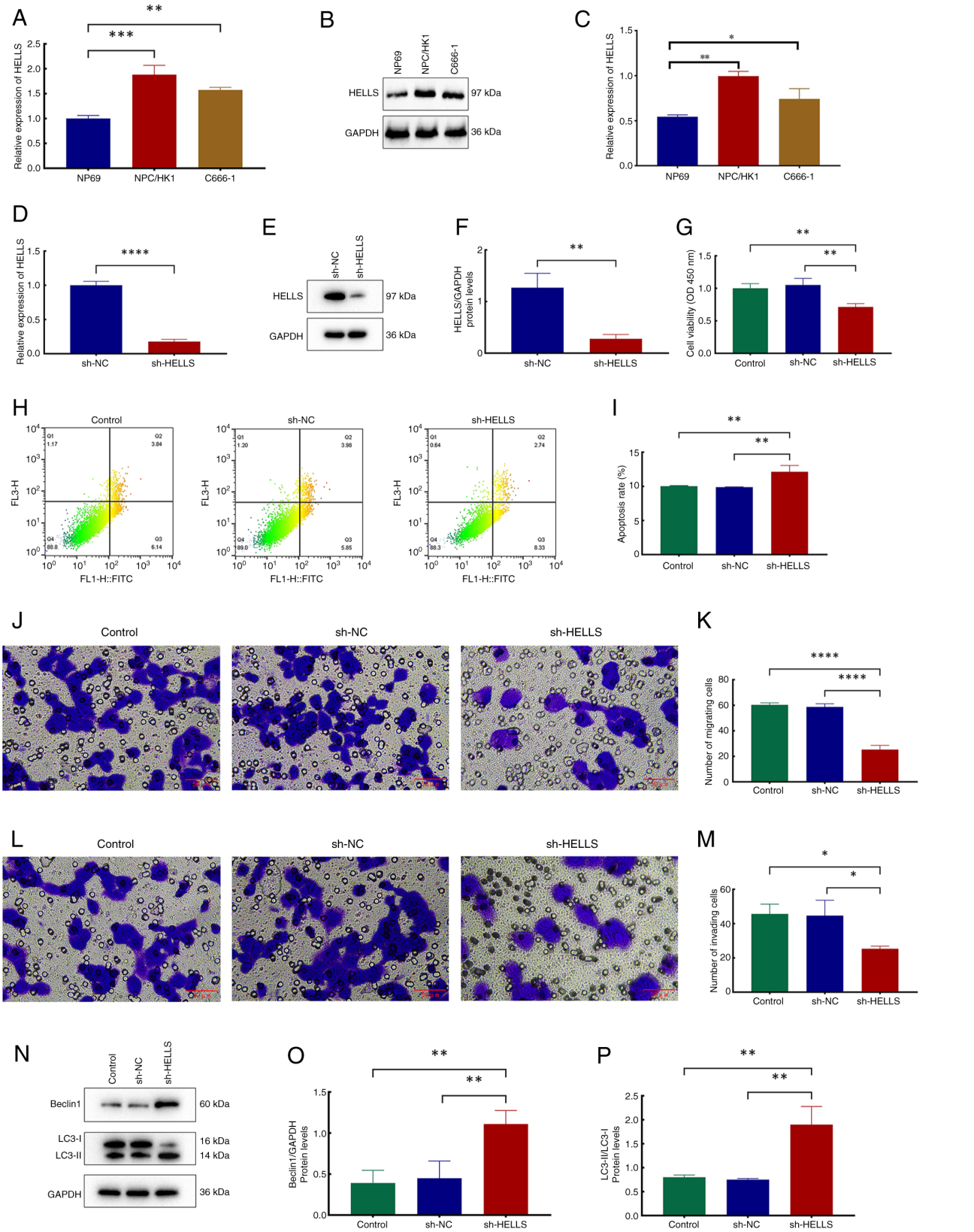

Figure 2. Exploration of the effects of HELLS on NPC *in vitro*. (A) Relative mRNA expression levels of HELLS in NPC cell lines NP69, NPC/HK1 and C666-1. (B) Representative images of protein blots of HELLS. (C) Relative protein expression levels of HELLS in the NPC cell lines NP69, NPC/HK1 and C666-1. (D) Relative mRNA expression levels of HELLS in the sh-NC and sh-HELLS groups. (E) Representative images of protein blots of HELLS. (F) Relative protein expression levels of HELLS in the sh-NC and sh-HELLS groups. (G) Relative viability of the control, sh-NC and sh-HELLS groups. (H) Flow cytometry plots of the control, sh-NC and sh-HELLS groups. (I) Analysis of cell apoptosis' rates across the three groups. (J) Representative images depicting crystal violet staining of migratory cells across the three groups. (K) Quantitative analysis of migratory cells across the three groups. (L) Representative images depicting crystal violet staining of invasive cells across the three groups. (M) Quantitative analysis of invading cells across the three groups. (N) Representative images of protein blots of beclin1, LC3-I and LC3-II. (O) Relative protein expression levels of beclin1 in the three groups. (P) Relative ratios of LC3-II to LC3-I protein expression levels in the three groups. *P<0.05, **P<0.01, ***P<0.001 and ****P<0.0001. HELLS, lymphoid-specific helicase; NPC, nasopharyngeal carcinoma; sh-, short hairpin; NC, negative control.

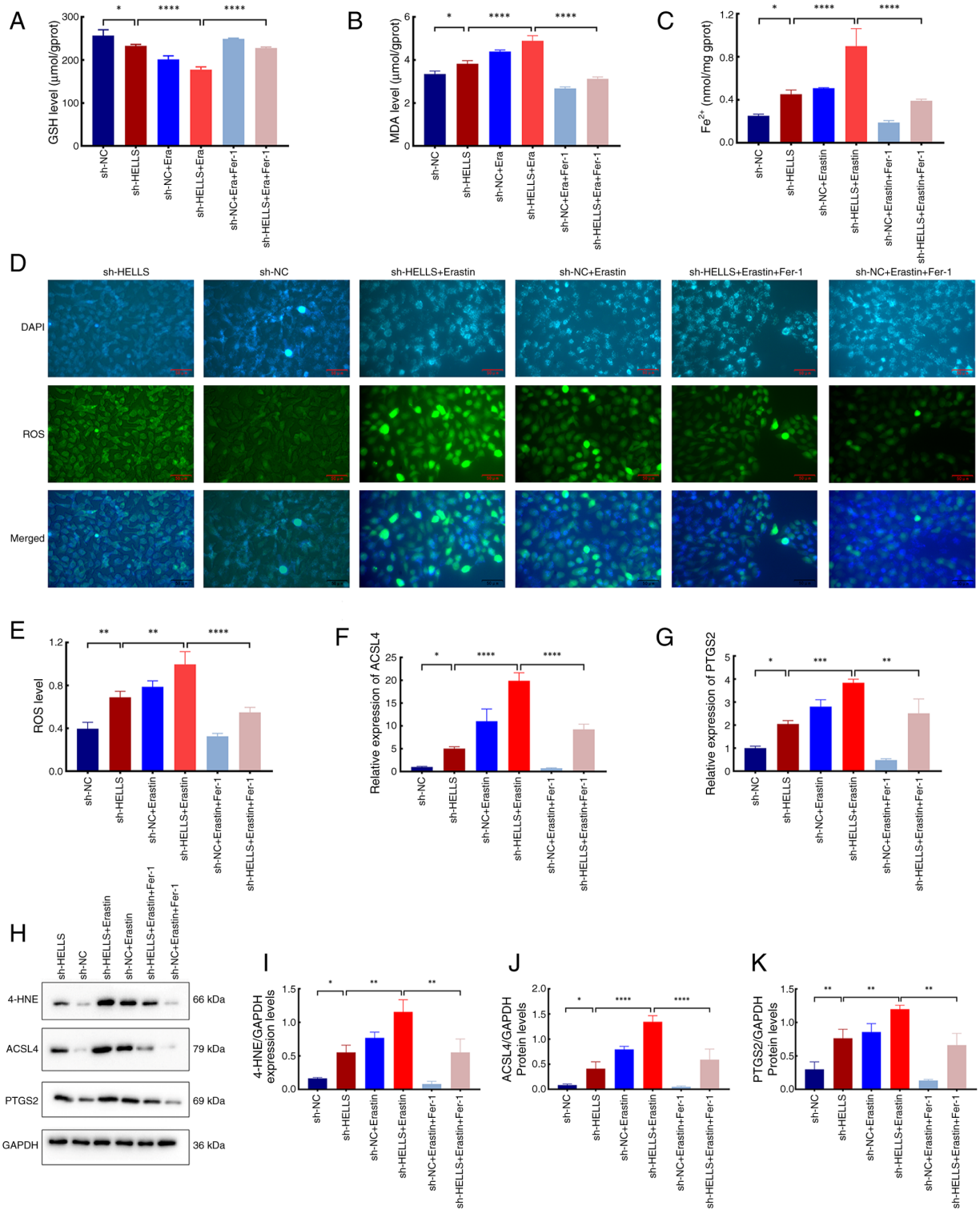

Figure 3. Effects of HELLS on ferroptosis. Levels of (A) GSH, (B) MDA and (C) Fe^{2+} in the sh-HELLS, sh-NC, sh-HELLS + Era, sh-NC + Era, sh-HELLS + Era + Fer-1 and sh-NC + Era + Fer-1 groups. (D) Representative images illustrating immunofluorescence staining of ROS probes in the six groups. (E) ROS levels in the six groups. (F and G) Relative mRNA expression levels of (F) ACSL4 and (G) PTGS2 in the six groups. (H) Representative images of immunoblots of 4-HNE, ACSL4 and PTGS2. (I) Relative expression levels of 4-HNE in the six groups. (J and K) Relative protein expression levels of (J) ACSL4 and (K) PTGS2 in the six groups. *P<0.05, **P<0.01, ***P<0.001 and ****P<0.0001. HELLS, lymphoid-specific helicase; GSH, glutathione; MDA, malondialdehyde; sh-, short hairpin; NC, negative control; Era, erastin; Fer-1, ferrostatin-1; ROS, reactive oxygen species; 4-HNE, 4-hydroxynonenal; ACSL4, acyl-CoA synthetase long-chain family member 4; PTGS2, prostaglandin-endoperoxide synthase 2.

HELLS inhibits autophagy-dependent ferroptosis. The role of HELLS in autophagy-dependent ferroptosis was subsequently investigated. Following erastin treatment, the autophagy agonist Rapa and inhibitor 3-MA were administered to sh-HELLS and sh-NC cells, and cell viability was assessed. The sh-HELLS group exhibited significantly lower cell viability than the sh-NC group (P<0.05; Fig. 4A). Furthermore, Rapa treatment significantly decreased cell viability, whereas

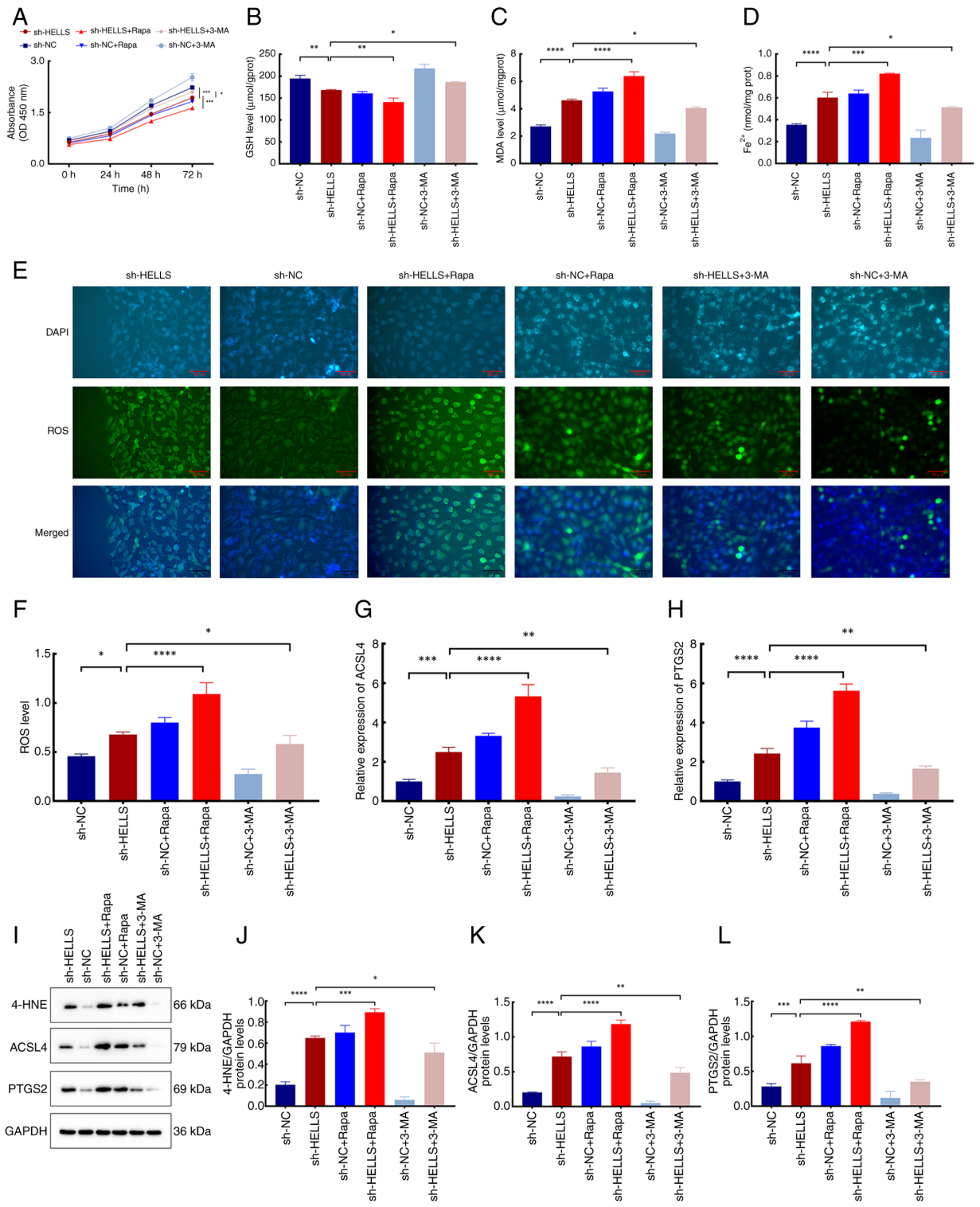

Figure 4. Effects of HELLS on autophagy-dependent ferroptosis. (A) Relative viability of the sh-HELLS, sh-NC, sh-HELLS + Rapa, sh-NC + Rapa, sh-HELLS + 3-MA, and sh-NC + 3-MA groups at 0, 24, 48 and 72 h. Levels of (B) GSH, (C) MDA and (D) Fe^{2+} in the six groups. (E) Representative images illustrating immunofluorescence staining of the ROS probes in the six groups. (F) ROS levels in the six groups. (G and H) Relative mRNA expression levels of (G) ACSL4 and (H) PTGS2 in the six groups. (I) Representative images of immunoblots of 4-HNE, ACSL4, and PTGS2. (J) Relative expression levels of 4-HNE in the six groups. Relative protein expression levels of (K) ACSL4 and (L) PTGS2 in the six groups. *P<0.05, **P<0.01, ***P<0.001 and ****P<0.0001. HELLS, lymphoid-specific helicase; sh-, short hairpin; NC, negative control; Rapa, rapamycin; 3-MA, 3-Methyladenine; GSH, glutathione; MDA, malondialdehyde; ROS, reactive oxygen species; 4-HNE, 4-hydroxynonenal; ACSL4, acyl-CoA synthetase long-chain family member 4; PTGS2, prostaglandin-endoperoxide synthase 2.

3-MA treatment counteracted this effect. This assessment preliminarily indicated that HELLS could inhibit ferroptosis via an autophagy-dependent mechanism.

To validate the enhanced role of HELLS in autophagy-dependent ferroptosis, GSH, MDA, Fe^{2+} and ROS were re-analyzed after Rapa or 3-MA treatments. The experimental

results demonstrated that under consistent experimental conditions, the levels of GSH in the sh-HELLS group were substantially reduced compared with those in the sh-NC group (Fig. 4B; P<0.05). Additionally, Rapa induced a significant reduction in GSH levels, whereas 3-MA substantially increased them (P<0.05). Conversely, the levels of MDA, Fe^{2+} and ROS in each cell group were inversely associated with those of GSH (Fig. 4C-F; P<0.05).

Moreover, expression levels of *ACSL4* and *PTGS2* were increased in the sh-HELLS group compared with those in the sh-NC group (P<0.05). Similarly, Rapa or 3-MA treatment resulted in the upregulation or downregulation of these genes, respectively (Fig. 4G and H; P<0.05). The expression patterns of the corresponding proteins aligned with those of their respective genes, as well as the consistent expression level of the biomarker 4-HNE (Fig. 4I-L; P<0.001 and P<0.0001). Undoubtedly, these findings provide compelling evidence that HELLS is crucial in inhibiting autophagy-dependent ferroptosis.

HELLS regulates autophagy-dependent ferroptosis through the Nrf2/HO-1/GPX4 signaling pathway. To uncover the role of HELLS in modulating ferroptosis via the Nrf2/HO-1/GPX4 signaling pathway, cells were treated with the Nrf2 activator ML334 following erastin treatment, and ferroptosis markers, as well as the pathway components, were assessed.

The Co-IP results indicated that there was an interaction between HELLs and Nrf2 (Fig. 5A). Cell viability assessment revealed that the sh-HELLS group had significantly lower cell viability than the sh-NC group (P<0.05). Nevertheless, following ML334 treatment, cell viability significantly enhanced, indicating that ML334 effectively mitigates the ferroptosis induced by HELLS knockout (Fig. 5B; P<0.05). Additionally, the levels of ferroptosis biomarkers (GSH, MDA and Fe^{2+}) were re-evaluated following ML334 treatment. Consistent with previous investigations, GSH levels significantly decreased after HELLS knockout, whereas MDA and Fe^{2+} levels comparatively increased (P<0.0001). Following ML334 treatment, GSH levels significantly increased, accompanied by a simultaneous decrease in MDA and Fe^{2+} concentrations in both cell groups, in comparison with pretreatment conditions (Fig. 5C and D; P<0.05).

To further elucidate the involvement of HELLS in the Nrf2/HO-1/GPX4 signaling pathway, the expression levels of associated genes and proteins were evaluated. As demonstrated in Fig. 5E-G, the expression levels of *Nrf2*, *HO-1* and *GPX4* genes were significantly downregulated in the sh-HELLS group (P<0.01). Furthermore, ML334 administration led to a substantial increase in the expression levels of these genes (P<0.05). Additionally, the protein levels of Nrf2, HO-1 and GPX4 were evaluated, revealing that their expression patterns in each cell group correspond with their respective gene expression profiles (Fig. 5H and I; P<0.05 and P<0.01). The aforementioned findings indicated that HELLS knockout significantly inhibits the Nrf2/HO-1/GPX4 signaling pathway, which acts as a critical regulator in the modulation of autophagy-dependent ferroptosis. Meanwhile, after knockdown of HELLS, the levels of Beclin1 and LC3 increased significantly (P<0.05); subsequent addition of ML334 led to a significant decrease in Beclin1 and LC3 (P<0.05). These findings indicated that HELLS influences the progression of NPC by regulating autophagy via Nrf2(Fig. 5J and K).

HELLS facilitates NPC progression by modulating the Nrf2/HO-1/GPX4 signaling pathway in vivo. *In vitro* studies have demonstrated that HELLS inhibits ferroptosis by modulating the Nrf2/HO-1/GPX4 signaling pathway, thereby facilitating NPC progression. To further validate this, *in vivo* investigations were also conducted. Initially, a tumorigenesis assay utilizing nude mice was conducted to establish a xenograft model of NPC (Fig. 6A and B). The data presented (Fig. 6C and D) clearly indicated that the tumor volume and weight in the sh-HELLS group were substantially reduced in comparison with those in the sh-NC group (P<0.05), further indicating that HELLS acts as a critical factor in promoting NPC development. Moreover, the expression level of HELLS was significantly reduced in the tumor tissue in the sh-HELLS group in comparison with that in the sh-NC group (Fig. 6E and F; P<0.01). Besides, mRNA and protein expression levels of the autophagy markers LC3 and Beclin 1 were significantly upregulated in tumors with suppressed HELLS expression, indicating a suppressive effect of HELLS on autophagy (Fig. 6G-K; P<0.05 and P<0.001).

Subsequently, the molecular mechanisms by which HELLS inhibits ferroptosis and promotes NPC progression were validated *in vivo*. The mRNA and protein expression levels of *GPX4*, *HO-1* and *Nrf2* genes were all significantly downregulated in the tumors of the sh-HELLS group compared with those of the sh-NC group (Fig. 6L-R; P<0.05 and P<0.01). The consistent expression patterns of genes and proteins associated with the Nrf2/HO-1/GPX4 signaling pathway observed both *in vivo* and *in vitro* provide compelling evidence that HELLS can inhibit ferroptosis and promote NPC progression through the modulation of this pathway.

Discussion

In contrast to other regions globally, China, particularly its southern provinces, has consistently been demonstrated as a high-incidence area for NPC. Although the incidence of this malignant carcinoma has declined in recent years, the current epidemiological landscape remains critically concerning and warrants substantial attention. Currently, the clinical treatment regimens commonly used for NPC include radiotherapy, chemotherapy, combined chemoradiotherapy and immunotherapy. However, their application is often limited by adverse reactions, drug resistance and other side effects (33-36). Therefore, investigating the pathogenesis of NPC and exploring novel therapeutic strategies remain the focus of current research. Despite research advancements, considerable uncertainties persist regarding the pathogenesis and progression of NPC, highlighting a substantial knowledge gap in various aspects of the disease. A comprehensive understanding of the pivotal genes and pathogenic mechanisms associated with NPC may greatly enhance the prevention and therapeutic strategies employed in clinical practice for this challenging condition.

In the present study, a bioinformatics analysis and a comprehensive literature review were conducted, which led to the selection and subsequent determination of the HELLS gene

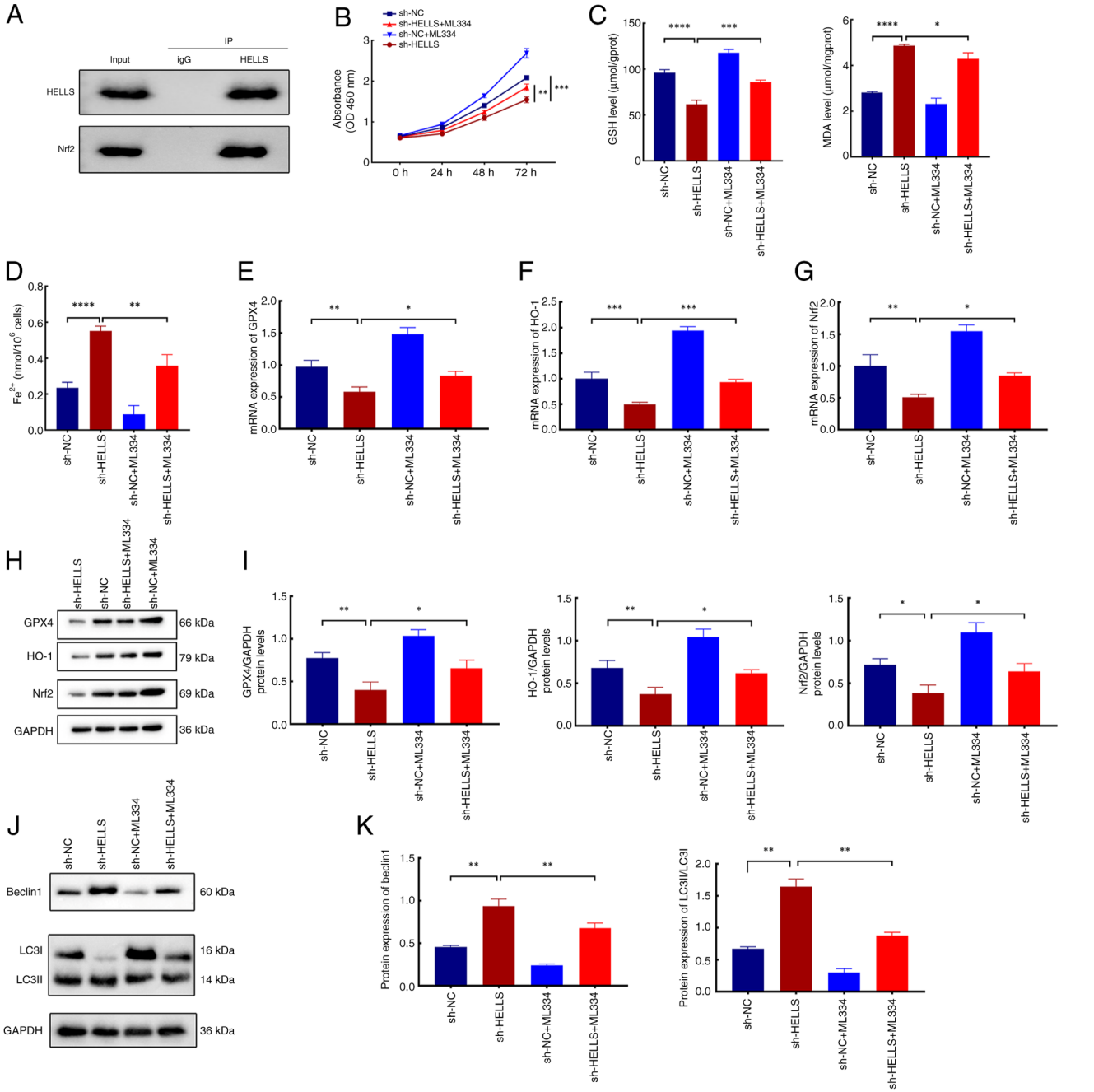

Figure 5. Mechanisms underlying the effects of HELLS on autophagy-dependent ferroptosis. (A) Co-immunoprecipitation was performed in HK-1 cells with either HELLS antibody or normal rabbit IgG antibody, followed by immunoblot analysis using the indicated antibodies. (B) Relative viability of the sh-HELLS, sh-NC, sh-HELLS + ML334 and sh-NC + ML334 groups at 0, 24, 48 and 72 h. Levels of (C) GSH, MDA and (D) Fe^{2+} in the four groups. (E-G) Relative mRNA expression levels of (E) GPX4, (F) HO-1 and (G) Nrf2 in the four groups. (H) Representative images of protein blots of GPX4, HO-1 and Nrf2. (I) Relative protein expression levels of GPX4 HO-1 and Nrf2 in the four groups. (J) Representative images of protein blots of Beclin1and LC3. (K) Relative protein expression levels of Beclin1and LC3 in the four groups. *P<0.05, **P<0.01, ***P<0.001 and ****P<0.0001. HELLS, lymphoid-specific helicase; sh-, short hairpin; NC, negative control; GSH, glutathione; MDA, malondialdehyde; GPX4, glutathione peroxidase 4; HO-1, heme oxygenase-1; Nrf2, nuclear factor-erythroid 2-related factor 2.

for in-depth investigation. This gene was hypothesized to play a significant role in NPC development. Through experimental validations, HELLS was found to function as an oncogene, playing a critical regulatory role in NPC and substantially promoting disease progression with high targeting specificity. This discovery can address the treatment gap for patients with advanced NPC or drug-resistant NPC who have high HELLS expression, providing a new direction for targeted therapy of NPC.

Not only in NPC, HELLS has been formally recognized to function as an oncogene in various cancers (29). The HELLS gene encodes a lymphoid-specific helicase, which has been widely acknowledged to function as a pivotal molecule in the maintenance of chromosome stability and DNA repair. Broadly acknowledged, DNA damage is a significant inducing factor in the etiology of cancers (37); therefore, DNA repair mechanisms exhibit pivotality in cancer progression, with significant contributions from the products encoded by the HELLS gene.

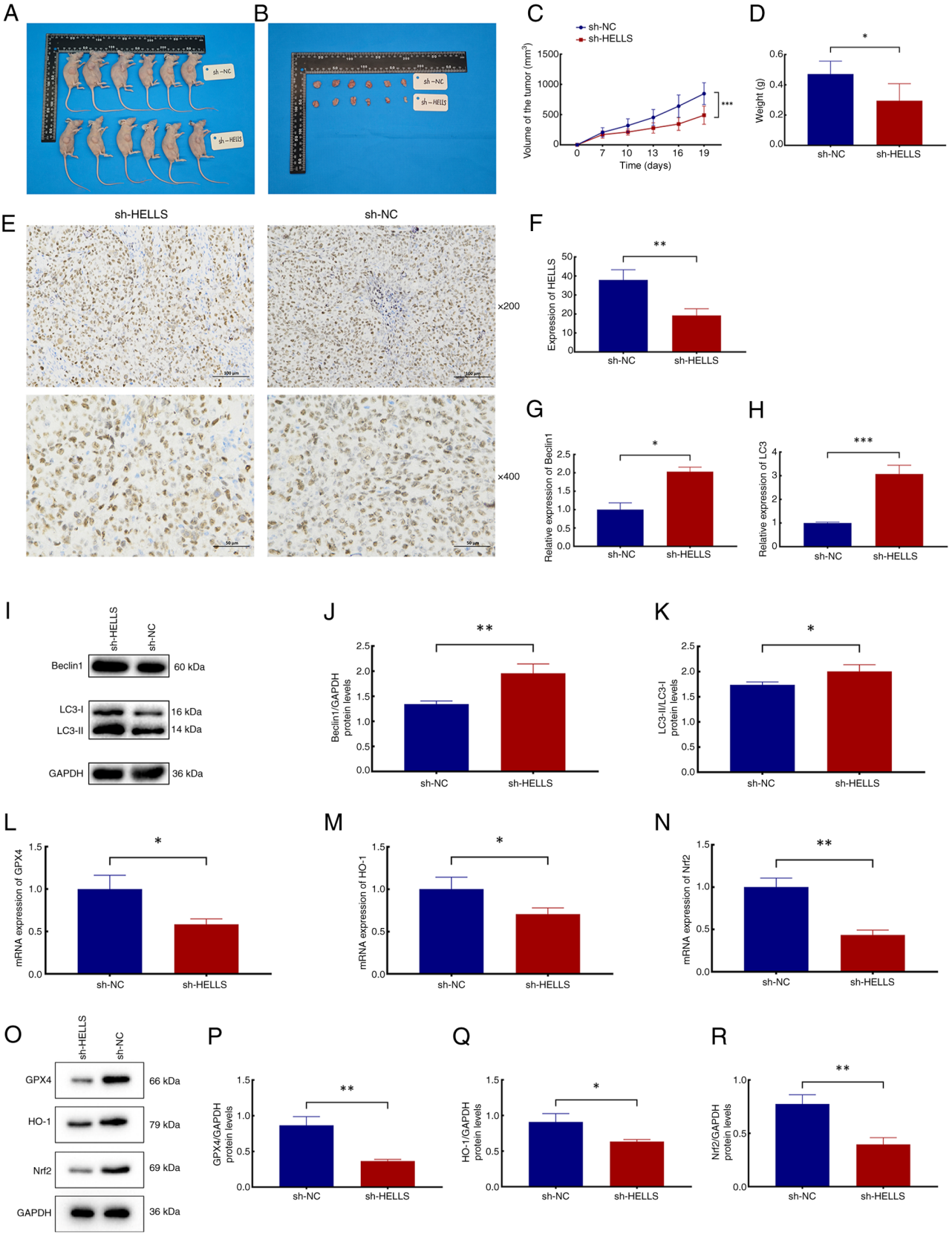

Figure 6. Effects of HELLS on autophagy-dependent ferroptosis and its mechanism *in vivo*. (A) Formation of subcutaneous nasopharyngeal carcinoma tumors in nude mice. (B) Tumors. (C) Volume of tumors in the sh-NC and sh-HELLS groups. (D) Weight of tumors in the two groups. (E) Representative images illustrating immunohistochemical staining of HELLS in tumors from the two groups (magnification, x200 and x400; scale bars, 100 or 50 μm). (F) Relative protein expression levels of HELLS in tumors from the two groups. (G and H) Relative mRNA expression levels of (G) beclin1 and (H) LC3. (I) Representative images of protein blots of beclin1, LC3-I and LC3-II. (J) Relative protein expression levels of beclin1 in the two groups. (K) Relative ratios of LC3-II to LC3-I protein expression levels in the two groups. (L-N) Relative mRNA expression levels of (L) GPX4, (M) HO-1 and (N) Nrf2 in tumors from the two groups. (O) Representative images of protein blots of GPX4, HO-1 and Nrf2. (P-R) Relative protein expression levels of (P) GPX4, (Q) HO-1 and (R) Nrf2 in tumors from the two groups. *P<0.05, **P<0.01 and ***P<0.001. HELLS, lymphoid-specific helicase; sh-, short hairpin; NC, negative control; GPX4, glutathione peroxidase 4; HO-1, heme oxygenase-1; Nrf2, nuclear factor-erythroid 2-related factor 2.

A study indicated that HELLS exhibited elevated expression across multiple cancers and may serve as a potential pan-cancer diagnostic and prognostic biomarker (28). Moreover, HELLS has been identified as a promising biomarker for pancreatic cancer (38,39), lung cancer (40) and hepatocellular carcinoma (41). Furthermore, Liu *et al* (30) indicated that HELLS was significantly upregulated in colorectal cancer, and its knockdown resulted in the arrest of the G2 and M cell cycle phases. In addition, HELLS facilitates the proliferation and self-renewal of glioma stem cells and interacts with E2F3 and MYC to regulate gene expression patterns in glioblastoma (42). In light of these significant findings regarding HELLS, HELLS is asserted to hold considerable promise as a therapeutic target for various cancers, including NPC.

Over more than a decade of extensive research, the inducing factors, mechanisms of occurrence, and roles of ferroptosis in various diseases have been redefined in light of its original discovery. A previous study indicated that ferroptosis requires the participation of autophagy (14). Subsequently, numerous studies have elucidated that autophagy-dependent ferroptosis constitutes a promising therapeutic target in cancer treatment (43), including glioblastoma (44) and colorectal cancer (45). In melanoma, Wang *et al* (46) demonstrated that the upregulation of the arachidonate 5-lipoxygenase (*ALOX5*) gene not only promotes autophagy and ferroptosis but also inhibits tumor progression. Given the substantial role of autophagy-dependent ferroptosis in cancer, the present study not only investigated the regulatory mechanisms through which HELLS influences ferroptosis but also examined its role in autophagy-dependent ferroptosis. By evaluating ferroptosis markers, in conjunction with the expression levels of *ACSL4* and *PTGS2* following treatment with ferroptosis agonist and inhibitor, as well as autophagy agonist and inhibitor, the present study provided substantial evidence that the HELLS gene significantly contributes to the inhibition of autophagy and ferroptosis in NPC cells. These findings indicate that HELLS may impede autophagy-dependent ferroptosis by downregulating autophagy in NPC cells. These findings are consistent with existing literature, highlighting the significance of autophagy-dependent ferroptosis in cancer.

Nrf2 functions as a transcription factor and belongs to a small family of basic leucine zipper proteins (47). This transcription factor is crucial in regulating the expression of genes related to the antioxidant stress response, including the *HO-1* gene (48), whose product is instrumental in safeguarding against oxidative damage, modulating cellular apoptosis, and mediating inflammatory responses (49). Researchers discovered that both Nrf2 and HO-1 can regulate the expression level of GPX4 (50), which encodes a distinct isoform of glutathione peroxidase, which has been recognized as a central inhibitor of ferroptosis (47,51). Thus, the Nrf2/HO-1/GPX4 signaling pathway is regarded as a crucial mechanism in ferroptosis regulation. Yang *et al* (22) indicated that Maresin-1 is protective against acute liver injury induced by ferroptosis through the stimulation of the Nrf2/HO-1/GPX4 pathway. Furthermore, Yang *et al* (20) revealed that polyphyllin I can induce ferroptosis in hepatocellular carcinoma cells by inhibiting the Nrf2/HO-1/GPX4 signaling pathway. In the present study, Co-IP experiments confirmed a physical interaction between HELLS and Nrf2. However, further verification through chromatin immunoprecipitation, stability analysis, and other assays is still needed to deepen our understanding of the regulatory effect of HELLS on Nrf2. Additionally, the present study further confirmed that the HELLS gene can inhibit autophagy-dependent ferroptosis in NPC cells by regulating the Nrf2/HO-1/GPX4 signaling pathway. Notably, based on existing findings, including the overexpression of HELLS in NPC, its role in promoting ferroptosis resistance, and its association with poor prognosis, it is considered that regulating HELLS through small molecule inhibitors or gene silencing technologies holds significant therapeutic potential in the treatment of NPC. The development of HELLS modulators is expected to become a potentially effective therapeutic strategy for NPC.

Currently, studies on the functional role of HELLS in NPC remain relatively limited. Immune escape and therapeutic resistance are key issues restricting the clinical efficacy of NPC treatment, yet their association with HELLS has not been explored. He *et al* (52) found that HELLS is highly expressed in NPC and can regulate cancer cell metabolism to support the epithelial-mesenchymal transition process, thereby promoting the malignant progression of NPC. Another study explored the interaction between HELLS and ferroptosis inducers, and the results showed that overexpression of HELLS can significantly inhibit the death of cervical cancer cells mediated by the ferroptosis inducer Erastin, suggesting that HELLS may play a key role in regulating the ferroptosis sensitivity of tumor cells (53). In addition, immune escape and therapeutic resistance of NPC have become research hotspots in the field. circBART2.2 promotes the transcriptional activation of PD-L1 by binding to RIG-1, ultimately leading to immune escape of tumor cells (54). Cai *et al* (55) found that in a hypoxic microenvironment, Erastin and its target molecule BAP1 may serve as effective intervention approaches to reduce the drug resistance of NPC. However, at present, the specific mechanism by which HELLS regulates immune escape and therapeutic resistance in NPC remains unclear, and further in-depth exploration and verification are required in subsequent studies.

There are certain limitations to the present study. First, the representativeness of samples and cell models is insufficient: The number of patient tumor samples is small, only two NPC cell lines (NPC/HK1 and C666-1) were used, and no normal nasopharyngeal epithelial cells were included as controls. Meanwhile, large-sample clinical follow-up data are lacking, making it impossible to clarify the association between HELLS and patient prognosis. In the future, it is necessary to expand the sample size, supplement external datasets, verify HELLS function in normal epithelial cells, and combine follow-up analysis to explore its prognostic value. Second, although it was confirmed that HELLS regulates ferroptosis through the Nrf2/HO-1/GPX4 pathway, the causal relationship between HELLS and this pathway has not been clarified, the role of HELLS in the downstream of the pathway has not been verified, and direct evidence for autophagic degradation of ferroptosis-related substrates is lacking. In *in vivo* experiments, neither ferroptosis markers were detected nor Nrf2 agonist rescue experiments were conducted. Subsequent studies need to supplement experiments such as rescue experiments and loss-of-function experiments to improve the mechanistic chain. Third, the safety and specificity of targeted intervention

have not been evaluated. Although shRNA-mediated HELLS knockdown verified target specificity, off-target effects have not been excluded, and the toxicity of targeted intervention on normal tissues has not been detected. In the future, it is necessary to use CRISPR-Cas9 and RNA-sequencing to verify specificity and conduct systematic toxicity assessment. Fourth, the exploration of research extension and clinical transformation value is insufficient. Other mechanisms by which HELLS regulates ferroptosis have not been deeply explored, and its role in the context of therapeutic resistance has not been analyzed. Subsequent plans include combining ferroptosis inducers, integrating tumor microenvironment analysis, and investigating the association between HELLS and drug resistance to provide insights for breaking through therapeutic bottlenecks.

In summary, the present study emphasizes the pivotal role of the HELLS gene in the regulation of NPC and autophagy-dependent ferroptosis. Findings of extensive research will deepen the understanding of the pathogenesis of NPC, thereby providing new insights for its precise clinical management. It is proposed that the HELLS gene holds considerable promise as a therapeutic target for NPC. Furthermore, the development of HELLS modulators is expected to become a viable therapeutic strategy for clinical application in NPC treatment, thereby contributing to the advancement of precision clinical treatments for this highly concerning disease.

In conclusion, HELLS can inhibit autophagy-dependent ferroptosis in NPC cells through the activation of the NRF2/HO-1/GPX4 signaling pathway, consequently facilitating NPC progression. The HELLS gene may represent a significant therapeutic target for NPC.

Acknowledgements

Not applicable.

Funding

The present study was supported by the Jilin Provincial Science and Technology Development Plan Project (grant no. 20240401069YY).

Availability of data and materials

The data generated in the present study may be requested from the corresponding author.

Authors' contributions

ZW and CJ designed the experiments. CJ and JL performed experiments and collected data. CJ and SH analyzed the data. CJ, CB and JY interpreted the data. All authors read and approved the final version of the manuscript. ZW and CJ confirm the authenticity of all the raw data.

Ethics approval and consent to participate

Waiver of informed consent and ethical approval for human studies (approval no. 2023-301) were granted by the Medical Ethics Committee of The Second Hospital of Jilin University (Changchun, China). Each animal experimental procedure gained approval from Institutional Animal Care and Use Committee of Jilin University (approval no. SY202406011; Changchun, China). The experimental protocol was performed in accordance with the relevant guidelines and regulations of the Basel Declaration. The study is reported in accordance with ARRIVE guidelines (https://arriveguidelines.org).

Patient consent for publication

Not applicable.

Competing interests

The authors declare that they have no competing interests.

References

1. Chen YP, Chan ATC, Le QT, Blanchard P, Sun Y and Ma J: Nasopharyngeal carcinoma. Lancet 394: 64-80, 2019.
2. Chang ET, Ye W, Zeng YX and Adami HO: The evolving epidemiology of nasopharyngeal carcinoma. Cancer Epidemiol Biomarkers Prev 30: 1035-1047, 2021.
3. Tang LL, Chen WQ, Xue WQ, He YQ, Zheng RS, Zeng YX and Jia WH: Global trends in incidence and mortality of nasopharyngeal carcinoma. Cancer Lett 374: 22-30, 2016.
4. Ding S, Gao Y, Lv D, Tao Y, Liu S, Chen C, Huang Z, Zheng S, Hu Y, Chow LK, *et al*: DNTTIP1 promotes nasopharyngeal carcinoma metastasis via recruiting HDAC1 to DUSP2 promoter and activating ERK signaling pathway. EBioMedicine 81: 104100, 2022.
5. Zhang B, Li J, Wang Y, Liu X, Yang X, Liao Z, Deng S, Deng Y, Zhou Z, Tian Y, *et al*: Deubiquitinase USP7 stabilizes KDM5B and promotes tumor progression and cisplatin resistance in nasopharyngeal carcinoma through the ZBTB16/TOP2A axis. Cell Death Differ 31: 309-321, 2024.
6. Liu H, Tang L, Gong S, Xiao T, Yang H, Gu W, Wang H and Chen P: USP7 inhibits the progression of nasopharyngeal carcinoma via promoting SPLUNC1-mediated M1 macrophage polarization through TRIM24. Cell Death Dis 14: 852, 2023.
7. Dixon SJ, Lemberg KM, Lamprecht MR, Skouta R, Zaitsev EM, Gleason CE, Patel DN, Bauer AJ, Cantley AM, Yang WS, *et al*: Ferroptosis: An iron-dependent form of nonapoptotic cell death. Cell 149: 1060-1072, 2012.
8. Tang D, Kang R, Berghe TV, Vandenabeele P and Kroemer G: The molecular machinery of regulated cell death. Cell Res 29: 347-364, 2019.
9. Li M, Jin S, Zhang Z, Ma H and Yang X: Interleukin-6 facilitates tumor progression by inducing ferroptosis resistance in head and neck squamous cell carcinoma. Cancer Lett 527: 28-40, 2022.
10. Li S, Liu Y, Li J, Zhao X and Yu D: Mechanisms of ferroptosis and application to head and neck squamous cell carcinoma treatments. DNA Cell Biol 40: 720-732, 2021.
11. Chen P, Wang D, Xiao T, Gu W, Yang H, Yang M and Wang H: ACSL4 promotes ferroptosis and M1 macrophage polarization to regulate the tumorigenesis of nasopharyngeal carcinoma. Int Immunopharmacol 122: 110629, 2023.
12. Chen Y, Feng Y, Lin Y, Zhou X, Wang L, Zhou Y, Lin K and Cai L: GSTM3 enhances radiosensitivity of nasopharyngeal carcinoma by promoting radiation-induced ferroptosis through USP14/FASN axis and GPX4. Br J Cancer 130: 755-768, 2024.
13. Zhou R, Qiu L, Zhou L, Geng R, Yang S and Wu J: P4HA1 activates HMGCS1 to promote nasopharyngeal carcinoma ferroptosis resistance and progression. Cell Signal 105: 110609, 2023.
14. Zhou B, Liu J, Kang R, Klionsky DJ, Kroemer G and Tang D: Ferroptosis is a type of autophagy-dependent cell death. Semin Cancer Biol 66: 89-100, 2020.
15. Miao H, Ren Q, Li H, Zeng M, Chen D, Xu C, Chen Y and Wen Z: Comprehensive analysis of the autophagy-dependent ferroptosis-related gene FANCD2 in lung adenocarcinoma. BMC Cancer 22: 225, 2022.
16. Liu J, Liu Y, Wang Y, Li C, Xie Y, Klionsky DJ, Kang R and Tang D: TMEM164 is a new determinant of autophagy-dependent ferroptosis. Autophagy 19: 945-956, 2023.

17. Chen YM, Xu W, Liu Y, Zhang JH, Yang YY, Wang ZW, Sun DJ, Li H, Liu B and Chen LX: Anomanolide C suppresses tumor progression and metastasis by ubiquitinating GPX4-driven autophagy-dependent ferroptosis in triple negative breast cancer. Int J Biol Sci 19: 2531-2550, 2023.
18. Gong G, Ganesan K, Liu Y, Huang Y, Luo Y, Wang X, Zhang Z and Zheng Y: Danggui Buxue Tang improves therapeutic efficacy of doxorubicin in triple negative breast cancer via ferroptosis. J Ethnopharmacol 323: 117655, 2024.
19. Du HF, Wu JW, Zhu YS, Hua ZH, Jin SZ, Ji JC, Wang CS, Qian GY, Jin XD and Ding HM: Fucoxanthin induces ferroptosis in cancer cells via downregulation of the Nrf2/HO-1/GPX4 pathway. Molecules 29: 2832, 2024.
20. Yang R, Gao W, Wang Z, Jian H, Peng L, Yu X, Xue P, Peng W, Li K and Zeng P: Polyphyllin I induced ferroptosis to suppress the progression of hepatocellular carcinoma through activation of the mitochondrial dysfunction via Nrf2/HO-1/GPX4 axis. Phytomedicine 122: 155135, 2024.
21. Zhu X, Chen X, Qiu L, Zhu J and Wang J: Norcantharidin induces ferroptosis via the suppression of NRF2/HO-1 signaling in ovarian cancer cells. Oncol Lett 24: 359, 2022.
22. Yang W, Wang Y, Zhang C, Huang Y, Yu J, Shi L, Zhang P, Yin Y, Li R and Tao K: Maresin1 protect against ferroptosis-induced liver injury through ROS inhibition and Nrf2/HO-1/GPX4 activation. Front Pharmacol 13: 865689, 2022.
23. Wen JY, Chen G, Li JD, Luo JY, He J, Wang RS and Qin LT: Downregulated miR-150-5p in the tissue of nasopharyngeal carcinoma. Genet Res (Camb) 2022: 2485055, 2022.
24. Luo X, Gong Y, Jiang Q, Wang Q, Li S and Liu L: Isoquercitrin promotes ferroptosis and oxidative stress in nasopharyngeal carcinoma via the AMPK/NF-κB pathway. J Biochem Mol Toxicol 38: e23542, 2024.
25. Yang T, Huang L, Qin H and Mai S: STRESS granule-associated RNA-binding protein CAPRIN1 drives cancer progression and regulates treatment response in nasopharyngeal carcinoma. Med Oncol 40: 47, 2022.
26. Wang Y, Yin W and Zhu X: Blocked autophagy enhances radiosensitivity of nasopharyngeal carcinoma cell line CNE-2 in vitro. Acta Otolaryngol 134: 105-110, 2014.
27. Li M, Wei Y, Liu Y, Wei J, Zhou X, Duan Y, Chen S, Xue C, Zhan Y, Zheng L, *et al*: BRD7 inhibits enhancer activity and expression of BIRC2 to suppress tumor growth and metastasis in nasopharyngeal carcinoma. Cell Death Dis 14: 121, 2023.
28. Liang X, Li L and Fan Y: Diagnostic, prognostic, and immunological roles of HELLS in pan-cancer: A bioinformatics analysis. Front Immunol 13: 870726, 2022.
29. Peixoto E, Khan A, Lewis ZA, Contreras-Galindo R and Czaja W: The chromatin remodeler HELLS: A new regulator in DNA repair, genome maintenance, and cancer. Int J Mol Sci 23: 9313, 2022.
30. Liu X, Hou X, Zhou Y, Li Q, Kong F, Yan S, Lei S, Xiong L and He J: Downregulation of the helicase lymphoid-specific (HELLS) gene impairs cell proliferation and induces cell cycle arrest in colorectal cancer cells. Onco Targets Ther 12: 10153-10163, 2019.
31. Chen X, Li Y, Rubio K, Deng B, Li Y, Tang Q, Mao C, Liu S, Xiao D, Barreto G and Tao Y: Lymphoid-specific helicase in epigenetics, DNA repair and cancer. Br J Cancer 126: 165-173, 2022.
32. Jia J, Shi Y, Chen L, Lai W, Yan B, Jiang Y, Xiao D, Xi S, Cao Y, Liu S, *et al*: Decrease in lymphoid specific helicase and 5-hydroxymethylcytosine is associated with metastasis and genome instability. Theranostics 7: 3920-3932, 2017.
33. Guan S, Wei J, Huang L and Wu L: Chemotherapy and chemo-resistance in nasopharyngeal carcinoma. Eur J Med Chem 207: 112758, 2020.
34. Wang C, Chen J, Su L, Hua Y, Ye J, Song X, Lv W, Zhang M, Huang F, Tian J and Hong J: The psychological status in patients with nasopharyngeal carcinoma during radiotherapy. Eur Arch Otorhinolaryngol 279: 1035-1042, 2022.
35. Huang H, Yao Y, Deng X, Huang Z, Chen Y, Wang Z, Hong H, Huang H and Lin T: Immunotherapy for nasopharyngeal carcinoma: Current status and prospects (Review). Int J Oncol 63: 97, 2023.
36. Xiao L, Kang W, Liao J and Li Y: Efficacy and tolerability of immunotherapy in advanced nasopharyngeal carcinoma with or without chemotherapy: A meta-analysis. Braz J Otorhinolaryngol 88 (Suppl 1): S70-S81, 2022.
37. Basu AK: DNA damage, mutagenesis and cancer. Int J Mol Sci 19: 970, 2018.
38. Hou X, Yang L, Wang K, Zhou Y, Li Q, Kong F, Liu X and He J: HELLS, a chromatin remodeler is highly expressed in pancreatic cancer and downregulation of it impairs tumor growth and sensitizes to cisplatin by reexpressing the tumor suppressor TGFBR3. Cancer Med 10: 350-364, 2021.
39. Wang FJ, Jing YH, Cheng CS, Cao ZQ, Jiao JY and Chen Z: HELLS serves as a poor prognostic biomarker and its downregulation reserves the malignant phenotype in pancreatic cancer. BMC Med Genomics 14: 189, 2021.
40. Zhu W, Li LL, Songyang Y, Shi Z and Li D: Identification and validation of HELLS (Helicase, Lymphoid-Specific) and ICAM1 (Intercellular adhesion molecule 1) as potential diagnostic biomarkers of lung cancer. PeerJ 8: e8731, 2020.
41. Fang Y, Tang W, Zhao D, Zhang X, Li N, Yang Y, Jin L, Li Z, Wei B, Miao Y, *et al*: Immunological function and prognostic value of lymphoid-specific helicase in liver hepatocellular carcinoma. Cancer Biomark 38: 225-239, 2023.
42. Zhang G, Dong Z, Prager BC, Kim LJ, Wu Q, Gimple RC, Wang X, Bao S, Hamerlik P and Rich JN: Chromatin remodeler HELLS maintains glioma stem cells through E2F3 and MYC. JCI Insight 4: e126140, 2019.
43. Liu L, Li L, Li M and Luo Z: Autophagy-dependent ferroptosis as a therapeutic target in cancer. ChemMedChem 16: 2942-2950, 2021.
44. Xie Y, Hou T, Liu J, Zhang H, Liu X, Kang R and Tang D: Autophagy-dependent ferroptosis as a potential treatment for glioblastoma. Front Oncol 13: 1091118, 2023.
45. Miao Q, Deng WQ, Lyu WY, Sun ZT, Fan SR, Qi M, Qiu SH, Zhu YR, Lin JP, Chen MF, *et al*: Erianin inhibits the growth and metastasis through autophagy-dependent ferroptosis in $KRAS^{G13D}$ colorectal cancer. Free Radic Biol Med 204: 301-312, 2023.
46. Wang M, Zeng G, Xiong B, Zhu X, Guo J, Chen D, Zhang S, Luo M, Guo L and Cai L: ALOX5 promotes autophagy-dependent ferroptosis by activating the AMPK/mTOR pathway in melanoma. Biochem Pharmacol 212: 115554, 2023.
47. Dang R, Wang M, Li X, Wang H, Liu L, Wu Q, Zhao J, Ji P, Zhong L, Licinio J and Xie P: Edaravone ameliorates depressive and anxiety-like behaviors via Sirt1/Nrf2/HO-1/Gpx4 pathway. J Neuroinflammation 19: 41, 2022.
48. Somparn N, Prawan A, Senggunprai L, Kukongviriyapan U, Jetsrisuparb A, Lee MH, Kim DH, Kukongviriyapan V and Surh YJ: Cellular adaptation mediated through Nrf2-induced glutamate cysteine ligase up-regulation against oxidative stress caused by iron overload in β-thalassemia/HbE patients. Free Radic Res 53: 791-799, 2019.
49. Ali T, Kim T, Rehman SU, Khan MS, Amin FU, Khan M, Ikram M and Kim MO: Natural dietary supplementation of anthocyanins via PI3K/Akt/Nrf2/HO-1 pathways mitigate oxidative stress, neurodegeneration, and memory impairment in a mouse model of Alzheimer's disease. Mol Neurobiol 55: 6076-6093, 2018.
50. Hayes JD and Dinkova-Kostova AT: The Nrf2 regulatory network provides an interface between redox and intermediary metabolism. Trends Biochem Sci 39: 199-218, 2014.
51. Brigelius-Flohé R and Flohé L: Regulatory phenomena in the glutathione peroxidase superfamily. Antioxid Redox Signal 33: 498-516, 2020.
52. He X, Yan B, Liu S, Jia J, Lai W, Xin X, Tang CE, Luo D, Tan T, Jiang Y, *et al*: Chromatin remodeling factor LSH drives cancer progression by suppressing the activity of fumarate hydratase. Cancer Res 76: 5743-5755, 2016.
53. Tie W and Ge F: Lymphoid-specific helicase inhibits cervical cancer cells ferroptosis by promoting Nrf2 expression. PeerJ 11: e16451, 2023.
54. Ge J, Wang J, Xiong F, Jiang X, Zhu K, Wang Y, Mo Y, Gong Z, Zhang S, He Y, *et al*: Epstein-barr virus-encoded circular RNA CircBART2.2 promotes immune escape of nasopharyngeal carcinoma by regulating PD-L1. Cancer Res 81: 5074-5088, 2021.
55. Cai W, Wu S, Lin Z, Ming X, Yang X, Yang M and Chen X: Hypoxia-induced BAP1 enhances erastin-induced ferroptosis in nasopharyngeal carcinoma by stabilizing H2A. Cancer Cell Int 24: 307, 2024.